Provided for non-commercial research and education use.
Not for reproduction, distribution or commercial use.

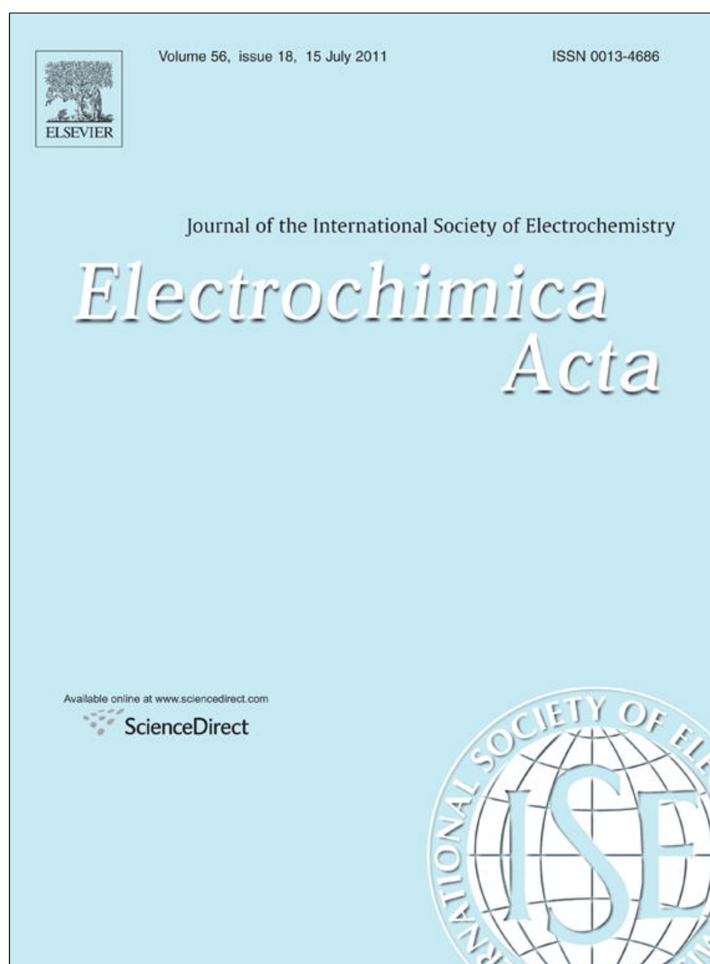

This article appeared in a journal published by Elsevier. The attached copy is furnished to the author for internal non-commercial research and education use, including for instruction at the authors institution and sharing with colleagues.

Other uses, including reproduction and distribution, or selling or licensing copies, or posting to personal, institutional or third party websites are prohibited.

In most cases authors are permitted to post their version of the article (e.g. in Word or Tex form) to their personal website or institutional repository. Authors requiring further information regarding Elsevier's archiving and manuscript policies are encouraged to visit:

http://www.elsevier.com/copyright

Author's personal copy

Electrochimica Acta 56 (2011) 6503–6509

Contents lists available at ScienceDirect

Electrochimica Acta

journal homepage: www.elsevier.com/locate/electacta

Doping saturation in dye-sensitized solar cells based on ZnO:Ga nanostructured photoanodes

Agnaldo S. Gonçalves [a,c], Márcio S. Góes [a], Francisco Fabregat-Santiago [b,*], Thomas Moehl [b], Marian R. Davolos [a], Juan Bisquert [b], Shozo Yanagida [d], Ana F. Nogueira [c], Paulo R. Bueno [a,*]

[a] Dpto. de Físico-Química, Instituto de Química de Araraquara, Universidade Estadual Paulista, R. Prof. Francisco Degni n. 55, 14800-900, Araraquara, SP, Brazil
[b] Grup de Dispositius Fotovotaics i Optoelectrònics, Departament de Física, Universitat Jaume I, Av. Sos Baynat, s/n, 12071, Castelló, Spain
[c] Institute of Chemistry, State University of Campinas, 13083-970, Campinas, SP, Brazil
[d] Center for Advanced Science and Innovation, Osaka University, Suita, Osaka, 565-0871, Japan

ARTICLE INFO

Article history:
Received 6 January 2011
Received in revised form 14 April 2011
Accepted 2 May 2011
Available online 7 May 2011

Keywords:
DSC
ZnO
Nanoparticles
Renewable energy
Electrochemical impedance spectroscopy

ABSTRACT

The origins of the performance of dye-sensitized solar cells based on ZnO:Ga nanostructured photoelectrodes, compared to analogous ZnO solar cells, were studied by means of impedance spectroscopy under illumination as a function of forward bias voltage. The film capacitance is governed by Ga doping. It can be assumed that the higher donor density of states of ZnO materials and, principally, ZnO:Ga-doped materials pin the Fermi level at a certain shallow energy level so that there is no photovoltage variation as a function of doping level. On the other hand, short circuit current is determined by the increasing roughness factor obtained at the higher doping levels while the lower fill factor values of DSCs based on ZnO:Ga, compared to analogous ZnO, were attributed to the higher ohmic resistive losses associated with the increasing photocurrent densities. In any case, the microstructure and morphological aspects were also considered as a possible origin of the low fill factor values. The estimated donor density level exceeds 10^{21} cm^{-3}, indicating a high doping level in the semiconductor. As a consequence of the synthesis process of ZnO:Ga nanoparticles its size diminishes with the higher Ga contents producing an increase in the overall roughness factor of the films, and then a larger dye upload and short circuit current.

© 2011 Elsevier Ltd. All rights reserved.

1. Introduction

Since Grätzel's group introduction in 1991 [1] dye-sensitized solar cells (DSCs) have been the focus of many investigations worldwide [2–5]. Basically, DSCs are built upon nanocrystalline semiconductor electrodes sensitized by a dye that absorbs the light and injects electrons into the conduction band of the semiconducting oxide (usually TiO_2) from which they reach the external circuit and a liquid redox system that regenerates the oxidized absorber. This type of solar cell offers low manufacturing costs without the necessity of high temperatures and vacuum during fabrication [6]. The best energy conversion efficiency reached so far is around 11–12% [7–9]. The main limitations to DSC efficiency are the large number of electrons that recombine with oxidized species from the redox system, energy mismatches between the HOMO of the dye and the redox species, and the trapping-limited diffusion of electrons as they are transported throughout the semiconductor porous nanostructure [10–13].

Among the semiconducting oxides used as photoanode, zinc oxide (ZnO) has been the object of much research for solar cell applications as an alternative to TiO_2. ZnO has a higher electronic mobility, similar electron affinity and energy level of the conduction band (3.4 and 3.2 eV, respectively) and can be doped both *n*-type and *p*-type [14,15]. Furthermore, ZnO photoanodes may be easily nanoarchitectured in a wide range of shapes (wires, tubes, stars, etc.) which should be able to improve light harvesting, electron transport and recombination properties leading to higher overall efficiencies [16–18]. Due to these favorable physicochemical properties several efforts have been made to prepare different nanostructured films. However, up to now the overall conversion efficiencies of ZnO-based DSCs are lower compared to those based on TiO_2 [19]. One of the reasons for the low efficiency of ZnO-based DSCs is attributed to excessive dye aggregation on the ZnO surface [20], which in turn causes slower electron injection from the dye to ZnO [21]. In addition to these, the conventional liquid electrolyte and the standard dyes are also known to be the causes of degradation in ZnO-based DSCs. Therefore optimization of these components is needed in order to obtain stable devices.

To enhance the electron transport properties in the ZnO nanostructured photoelectrode, Ga^{3+} was used in this work as a doping impurity. In gallium-doped zinc oxide (ZnO:Ga), Ga^{3+} is expected

* Corresponding authors.
E-mail addresses: fran.fabregat@fca.uji.es (F. Fabregat-Santiago), prbueno@iq.unesp.br (P.R. Bueno).

0013-4686/$ – see front matter © 2011 Elsevier Ltd. All rights reserved.
doi:10.1016/j.electacta.2011.05.003

Author's personal copy

to cause just a small lattice distortion due to the similar tetrahedral radii of Zn^{2+} and Ga^{3+} [22]. Ga^{+3} introduction into the ZnO matrix can introduce donor defects by means of Ga^{3+} substituting Zn^{2+}, increasing the charge carrier concentration and thus the electrical conductivity up to one order of magnitude [23]. We present here evidence of improved transport properties.

The study of recombination or charge transfer processes and the capacitive charging of ZnO photoelectrodes during operational conditions are crucial to correct possible malfunctions and for increasing the efficiencies of ZnO-based DSCs. The charge lifetime and/or recombination resistance are capable to be followed by transient techniques [24,25]. One example of a technique that can be used to calculate the charge lifetime is Stepped Light-Induced Transient Measurements of Photocurrent and Voltage (SLIM-PCV) [24]. However, transient techniques are not able to separate the contributions of recombination resistance and capacitance to the charge lifetime [26]. Impedance Spectroscopy (IS) has proven to be a powerful technique to investigate and determine charge transfer processes and electrochemical or chemical capacitance in DSCs [27–30]. Electron recombination at the semiconductor–electrolyte interface and the diffusion of the redox species in an electrolyte can be well distinguished in the spectral shapes of IS analysis [27–30].

In this paper, we study the effect of Ga doping on the capacitance and charge transfer resistance of ZnO-based DSCs by means of IS. We found that, upon doping, the capacitance follows a Mott–Schottky behavior that is indicative of the high donor density (>10^{21} cm^{-3}) attained by ZnO:Ga. The increase of the density of states induced by creation of shallow donor states due to Ga doping, causing saturation on the film capacitance was analyzed. It was found that from certain Ga concentration, donor density does not change proportionally to Ga contents, indicating that the ZnO structure saturates of Ga. We also found a nearly constant photopotential for all the samples and an increase of current associated to the increase of samples roughness at the higher dopant content.

2. Experimental

The ZnO films were prepared according to a previous work [31]. ZnO and ZnO:Ga with 1, 3, and 5 atomic % nanoparticles were synthesized by adapting a procedure described in the literature [32]. A zinc nitrate aqueous solution (0.1 mol L^{-1} at pH 5) was mixed with 0.1 mol L^{-1} triethanolamine. Gallium nitrate was used as the source of Ga^{3+}. The slurry was prepared by mixing ZnO or ZnO:Ga powder, deionized water, acetylacetone and a non-ionic surfactant (Triton X-100). The resulting mixture was ground in a mortar for ca. 1 h. The paste was used for the deposition of films onto conducting FTO-glass substrates by the doctor blade technique using adhesive tape (Scotch®) in order to control the photoelectrode film thickness. The semiconductor films were then heated at 450 °C for 30 min to provide adequate electrical contact between the particles. The resulting film thickness was 6 μm, measured by using a profiler (Sloan Technology, Dektak 3). The ZnO electrodes, while still warm (ca. 80 °C), were immersed for 3 h at room temperature in a 0.5 mmol L^{-1} solution of cis-bis(isothiocyanato)bis(2,2′-bipyridyl-4,4′-dicarboxylato)-ruthenium(II) bis-tetrabutylammonium (also known as N-719, used as received from Solaronix) in absolute ethanol. Then, the sensitized films were rinsed with absolute ethanol to remove non-adsorbed N-719 species and allowed to dry in air. The liquid electrolyte for DSCs was composed of 0.1 mol L^{-1} LiI, 0.05 mol L^{-1} I_2, 0.8 mol L^{-1} tetrabutylammonium iodide, 0.5 mol L^{-1} 4-tertbutylpyridine in acetonitrile and 3-methoxypropionitrile (50:50 in volume). A Pt-coated FTO-glass was used as the counter electrode. The Pt counter electrode and the working electrode were assembled in a sealed sandwich-type solar cell by heating with a hot-melt of the ionomer film Himilan (Mitsui-Dupont Polychemicals) as a spacer between the electrodes. The cell area was 0.15 cm^2.

Table 1
General data for DSCs based on ZnO, ZnO:Ga at 1, 3 and 5 atomic % nanostructured photoanodes under one sun illumination. V_{OC} is the open-circuit potential, j_{SC} the photocurrent, FF the fill factor, η the efficiency and β is the transfer factor calculated from Eq. (2).

Sample	ZnO	ZnO:Ga 1%	ZnO:Ga 3%	ZnO:Ga 5%
Particle diameter (nm)	120	70	60	40
Porosity (%)	15	39	55	58
Specific area ($m^2\,g^{-1}$)	9.6	17.6	25.4	33.8
DSC area (cm^2)	0.15	0.15	0.15	0.15
ZnO film thickness (μm)	6	6	6	6
Roughness factor	270	360	385	470
V_{OC} (V)	0.785	0.790	0.794	0.797
j_{SC} ($mA\,cm^{-2}$)	2.07	5.32	5.56	6.49
FF	0.46	0.33	0.38	0.37
η (%)	0.75	1.39	1.68	1.91
β	0.23	0.26	0.28	0.27
Donor density (cm^{-3})	–	1.4×10^{21}	2.5×10^{21}	2.9×10^{21}

The roughness factor was calculated according to the IUPAC definition [33], from the IUPAC compendium of Chemical Terminology where roughness factor is defined as $r_f = A_r/A_g$, where A_r is the real (true, actual) surface (interface) area and A_g is the geometric surface (interface) area. The specific surface area ($m^2\,g^{-1}$) obtained from BET analysis was used to estimate A_r after the calculation of the real amount of ZnO (in grams) in the volume of the photoanodes (geometrical area of the electrode multiplied by its thickness) corrected by the porosity values and considering the ZnO theoretical density of 5.6 g cm^{-3}. Table 1 summarizes the results obtained. It is important to emphasize that some authors [34] define roughness factor as the ratio between A_r and film thickness. Considering this definition one can obtain different values but herein we will be only concerned with the tendency of these values as a function of Ga doping and we are not concerned with the absolute value of r_f.

The impedance spectroscopy measurements were carried out by using a Solartron potentiostat (model SI1287) coupled to a frequency response analyzer (FRA module). The impedance spectra from the sealed DSCs were measured in a two-electrode configuration under illumination (AM1.5, 100 mW cm^{-2} by using the Yamashita Denso, YSS-80 solar simulator) at different bias voltages (including open-circuit voltage) with 10 mV AC perturbation over a frequency range of 100 kHz to 10 mHz. Data were fitted using the equivalent circuit model described in Fig. 4 [35].

3. Results and discussion

3.1. j–V characteristics

The j–V curves and the parameters of dye solar cells based on 6 μm thick pristine and Ga doped ZnO films are presented in Fig. 1 and Table 1.

From these results we observe as general trends that all the cells present very close values of the open circuit potential and very low values of the FF, while short circuit current increases, almost linearly with the Ga content.

The rise in j_{SC} with Ga content may be explained by the larger surface of semiconductor available for dye loading: the increasing concentration of Ga yields a decrease in the nanoparticles final size, providing an increase in the specific area of DSCs photoanodes. Fig. 2 illustrates the quasi-linear relationship between current density and roughness factor.

We will use impedance spectroscopy data to elucidate the origin of the low fill factor and the common V_{OC} in the solar cells.

Author's personal copy

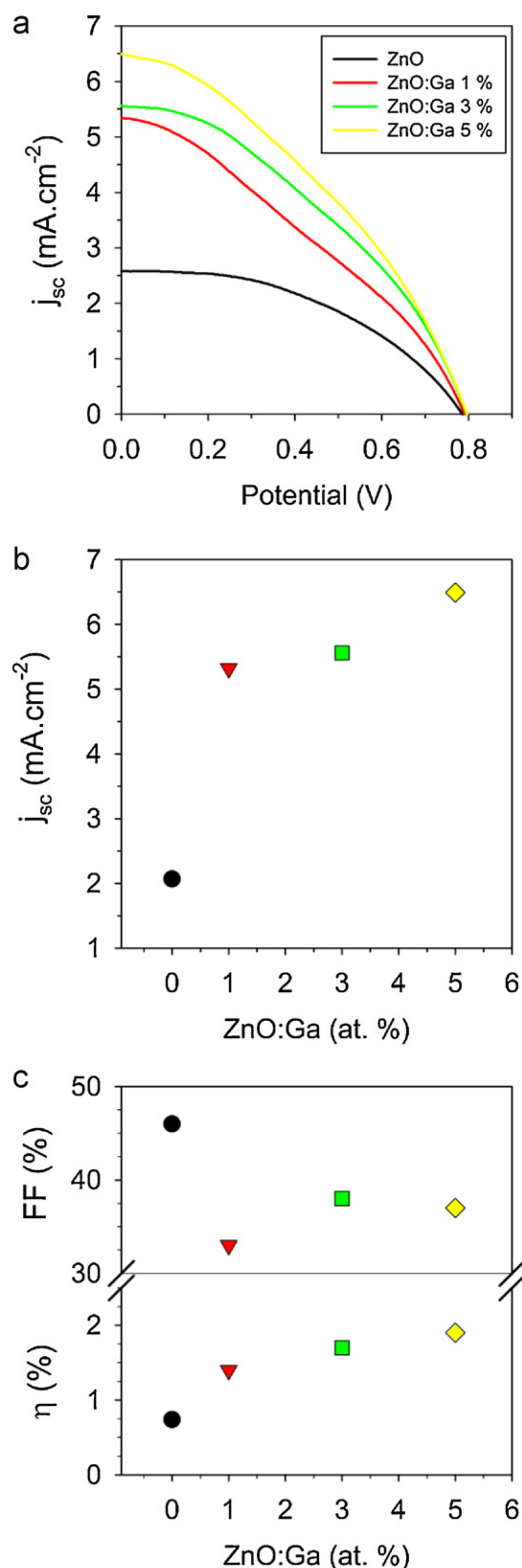

Fig. 1. (a) *j–V* curves obtained from the potentiostat (lines) and simulated from impedance values (dots). Parameters related to the performance of ZnO and ZnO:Ga-based DSCs: (b) short-circuit photocurrent density, (c) fill factor (empty symbols) and efficiency (full symbols).

3.2. Impedance analysis

The impedance spectra of the DSCs based on ZnO and ZnO:Ga photoelectrodes measured under one sun light intensity at forward bias voltages of 0.20, 0.40 and 0.60 V are shown in Fig. 3.

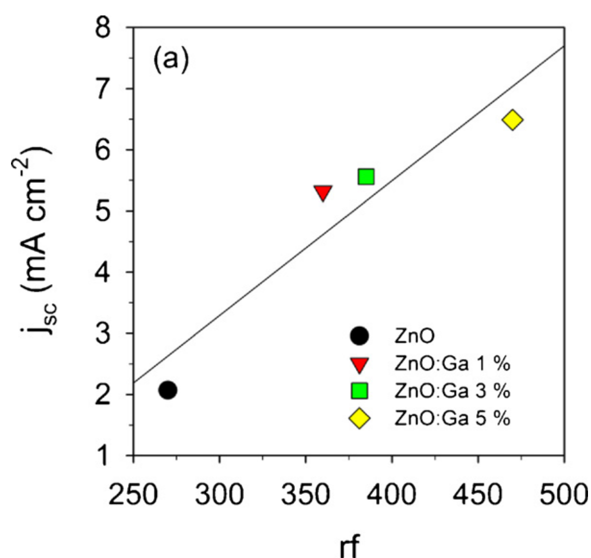

Fig. 2. Representation the roughness factor vs. current density in pure and increasingly Ga doped ZnO.

In general, a transmission line equivalent circuit model is used to model DSC response which consist of a series of distributed elements along the thickness, *L*, of the semiconductor nanostructure as shown in Fig. 4(a) [27–30]. We have used this equivalent circuit to fit data of pristine ZnO. For the ZnO:Ga samples and due to their high electronic conductivity, the electron transport resistance in the ZnO becomes negligible and the model of Fig. 4(a) is simplified to the one presented in Fig. 4(b).

The more relevant aspects of the impedance spectra of Fig. 3 are: (i) The high frequency semicircle (relaxation process), which is assigned to the charge transfer taking place at the electrolyte/counter electrode interface, i.e. to the injection of electrons in the electrolyte by means of the reduction of I_3^- ionic species into I^-. This kinetic process is associated to a charge transfer resistance, R_{Pt}, connected in parallel to the interfacial capacitance of the counter electrode, C_{Pt}, as illustrated in Fig. 4. (ii) The low frequency semicircle of the Nyquist impedance diagram of Fig. 3 which is attributed to the charge transfer resistance associated with the electron recombination process at the semiconductor/electrolyte interface that is in parallel with the film capacitance of electrons in the nanostructured photoelectrode, as sketched in Fig. 4(b).

The effect of Ga doping on R_{rec} and C_F were studied separately by means of the evaluation of the low frequency semicircle of the spectra given in Fig. 3.

3.3. Recombination analysis

The charge transfer resistance arising at the porous nanostructured electrode in contact with liquid electrolyte may be described by using a recombination resistance, R_{rec}, that depends on the potential as:

$$R_{rec} = R_0 \exp\left[\beta \frac{E_{redox} - E_{Fn}}{k_B T}\right] \quad (1)$$

where R_0 is a constant indicating the onset of recombination, β is the transfer factor governing the recombination, k_B is the Boltzmann constant, T the temperature, E_{Fn} the Fermi level of electrons in the semiconductor and E_{redox} the redox potential (i.e., the Fermi level of holes in the electrolyte) which are related with the potential drop at the semiconductor film through $V_F = (E_{redox} - E_{Fn})/q$, with q the electron charge. In general, to obtain V_F it is needed to correct the applied potential from the series resistance drop [27–30].

Author's personal copy

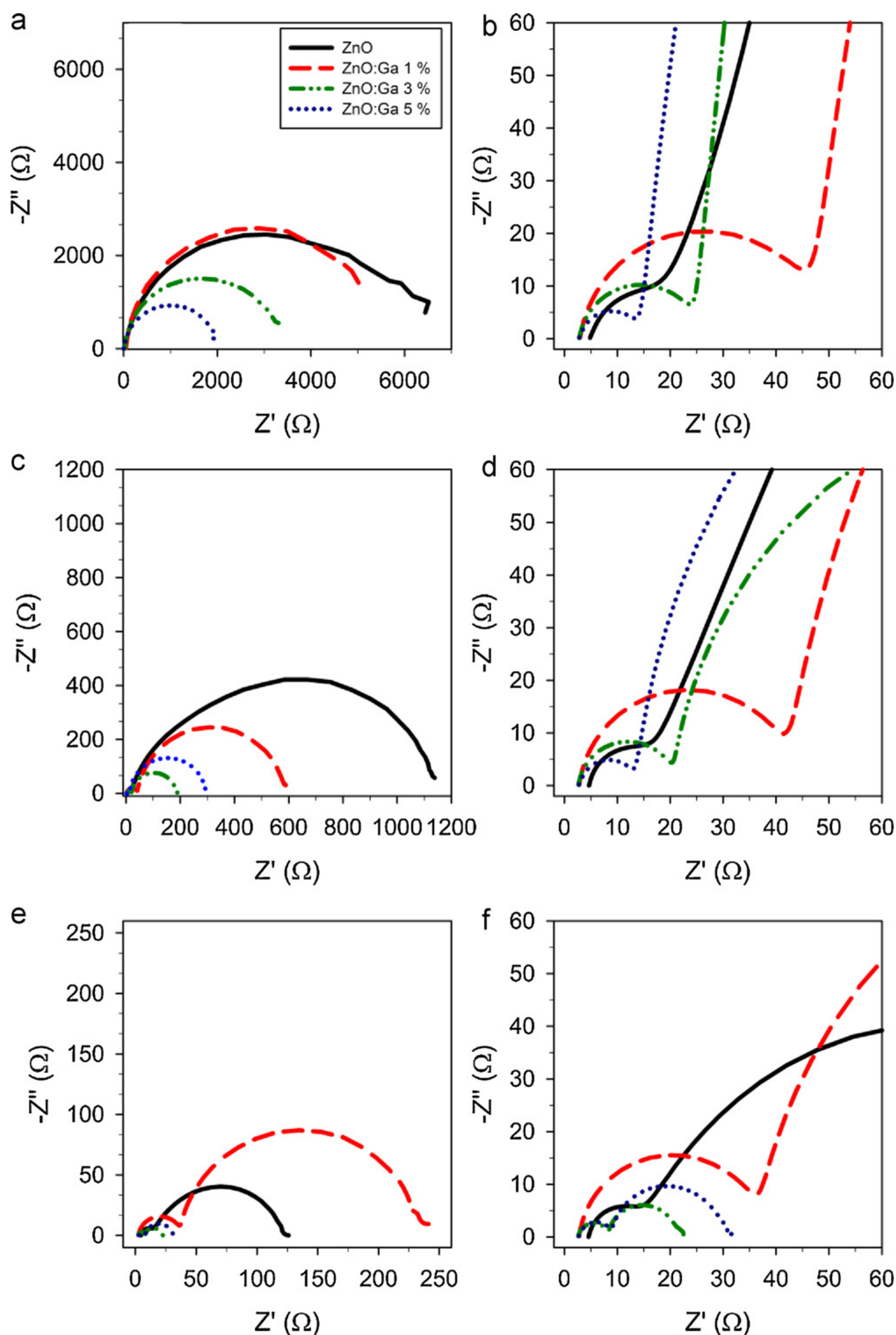

Fig. 3. Nyquist impedance diagrams of sealed DSCs based on ZnO and ZnO:Ga photoelectrodes (6-μm thick) at 1 sun (AM1.5) light intensity and different applied bias: (a) 0.20 V, (c) 0.40 V and (e) 0.6 V (d) forward bias. Two semicircles dominate the impedance: The smaller arc at high frequency is ascribed to the combination of the charge transfer resistance and the interfacial capacitance at the counter electrode/electrolyte interface. The larger arc appearing at low frequency is attributed to the charge transfer resistance associated with electron recombination at the interface, combined with the capacitance of electrons in the ZnO. The figures (b), (d) and (f) represent enlargement of the area at high frequency.

Fig. 5(a) shows that the recombination resistance is lower in doped samples than in undoped nanostructured ZnO photoanodes with respect to the Fermi level energy. For the pristine and ZnO:Ga up to a 3% doping, these differences may be related to the change in roughness of the surface obtained from BET measurements as described in Section 2, that lowers R_0 in Eq. (1). In the case of the ZnO prepared with a 5% of Ga, however, R_{rec} is nearly the same as the sample with 3% and this similarity also occurs in the capacitance shown in Fig. 5(b), even though according to BET measurements, the specific area of the 5% sample is 25% higher than the 3% doped one. As it will be described in more detail later, this effect is attributed to a saturation of Ga doping in ZnO. The spare Ga segregates at the surface of the ZnO grains of polycrystalline films, creating a barrier that blocks

Author's personal copy

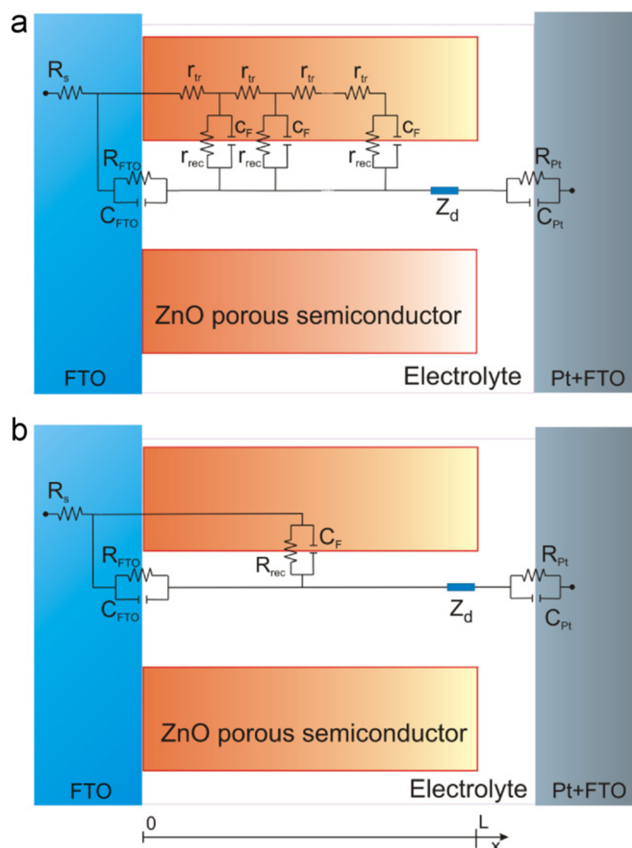

Fig. 4. (a) Transmission line model used for the description of low-doped nanostructured films. (b) Simplification of the previous model for samples presenting a high conductivity. r_{tr} is the transport resistance in the semiconductor, r_{rec} and c_F ($R_{rec} = r_{rec}/L$ and $C_F = C_F L$) are respectively the charge transfer resistance and film capacitance, Z_d is the Warburg element showing the Nernst diffusion of I_3^- in the liquid electrolyte. R_{Pt} and C_{Pt} are the charge transfer resistance and double-layer capacitance at the counter electrode (platinum chemically coated on TCO glass, indicated in the figure as TCO + Pt). R_{TCO} and C_{TCO} are the charge transfer resistance and the corresponding capacitance at the exposed TCO/electrolyte interface.

both recombination and also the increase of capacitance [36]. Indeed, phase segregation in ZnO:Ga powder samples, especially those with a higher Ga content, has been observed previously [22].

From the slope of these R_{rec} curves in Fig. 5(a), the transfer factor (β) is easily determined, see Table 1 [30]. It is important to notice that the values obtained for β are very low in comparison to those found for TiO_2, which use to be larger than 0.5 [30]. The slight increase of β for doped samples suggests a change in the recombination mechanism associated with the introduction of Ga ions in the semiconductor structure and eventually with the segregation of Ga excess.

A priori, the value of R_{rec} could be affected by the contribution for the recombination from the uncovered FTO in contact with the electrolyte, since no compact ZnO or TiO_2 underlayer (also known as blocking layer) was employed in the present work. However, we expect that this contribution becomes negligible even at low potentials, due both to the relatively small charge transfer rate from FTO to triiodide and the much larger area available for recombination from the nanostructured film.

3.4. Capacitance analysis

In semiconductors immersed in electrolytes containing a supporting salt, the charge carriers present in the solid phase can be compensated by the ionic charges in the electrolyte. If the

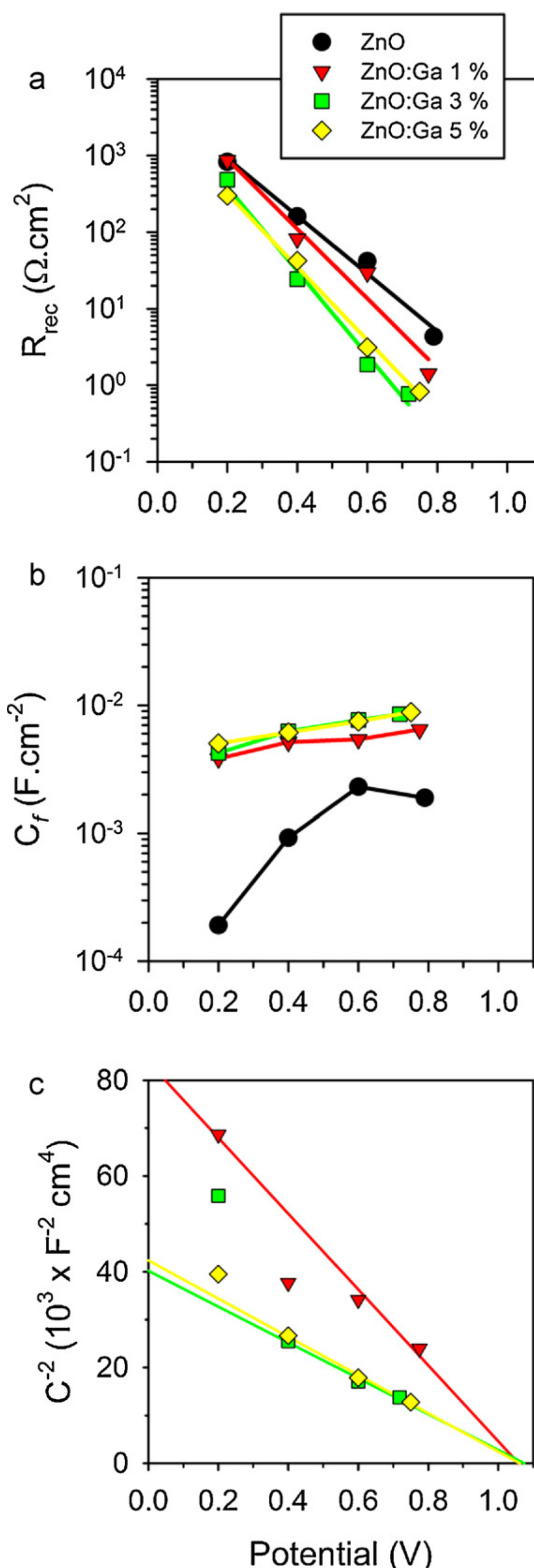

Fig. 5. (a) Recombination resistance (R_{rec}), (b) film capacitance (C_F) and (c) Mott–Schottky pattern of the film capacitance represented vs. the potential corrected from ohmic drop. The parameters were achieved by fitting the impedance data from DSCs based on ZnO and ZnO:Ga photoelectrodes.

Author's personal copy

semiconductor is nanostructured and poorly doped (pure or not intentionally doped), the variation of the applied potential produces an equivalent Fermi level shift, E_{Fn}, that sweeps the density of electronic states (DOS) modifying the capacitance, that in these conditions is termed *chemical capacitance* [37].

Thus, the chemical capacitance is a useful parameter to infer information on the DOS of the nanostructured photoanode with respect to E_{Fn}. For a potential such that $E_{Fn} << E_c$, where E_c is the conduction band energy, the chemical capacitance is related to the exponential density of bandgap sates [37,38]:

$$C_\mu = \frac{N_c q^2}{k_B T} \exp\left[-\frac{\alpha(E_c - E_{Fn})}{k_B T}\right] \quad (2)$$

with $\alpha = T/T_0$ a factor that describes the depth of trap states below the conduction band. N_c is the total density.

For highly doped semiconductor films, the capacitance is a combination of different contributions: in the semiconductor, the conduction band may bend even for very small nanoparticles. In the semiconductor the capacitance is then dominated by the depletion layer, C_{dl}, which follows a Mott–Schottky behavior [36,39]. In the electrolyte, the capacitance is dominated by the Helmholtz capacitance C_H which may be considered constant. Therefore the total film capacitance is the series combination of both: $C_F = (1/C_{dl} + 1/C_H)^{-1}$ with the smaller of them dominating C_F behavior [36]. From the analysis of capacitance as a function of potential it is possible to know the nature of the capacitance that domains the response.

Data shown in Fig. 5(b) suggest that, in the case of the pristine ZnO electrode the capacitance is dominated by the chemical capacitance contribution of ZnO, until it saturates at 0.6–0.8 V, while in the case of doped samples, the capacitance is dominated by the depletion layer inside the semiconductor nanoparticles.

In the case of pristine ZnO, we obtain a value of $\alpha = 0.20$. This value yields $T_0 = 1365$ K, which is large in comparison to common values of T_0 observed for TiO_2 nanostructured photoanodes which are comprised between 800 and 1200 K [26,28]. This result suggests a distribution of trap states extending to deeper levels below the conduction band in ZnO films. Very similar α values (ca. 0.2) were also found from the dependence, previously observed by SLIM-PCV, between the diffusion coefficient and electron density for DSCs based on pristine ZnO and ZnO:Ga photoanodes [24].

Confirmation of the behavior as depletion layer capacitance in doped samples is obtained when drawing a Mott–Schottky plot with data from the capacitance, Fig. 5(c). Estimating the roughness factor (r_f, see Section 2) of the film, it is possible to calculate the donor density through

$$N_d = \frac{2}{sq\varepsilon_r\varepsilon_0 r_f^2} \quad (3)$$

where s is the slope of the Mott–Schottky plot, $\varepsilon_r = 10$ is the dielectric constant of ZnO and ε_0 the permittivity of free space.

Despite limitations in the accuracy of the calculation of r_f, the values obtained for samples ZnO:Ga 1% and 3% were used as reference to have an estimation of N_d, providing donor density values of the order of 10^{21}, as presented in Table 1. The value of N_d obtained at 3% doping nearly doubles that for the 1% sample. As indicated above, data from recombination indicate that for the sample ZnO:Ga 5% a relevant part of the contact area between the semiconductor and the electrolyte is blocked. Therefore, for the calculation of the value of N_d in this sample, the value of r_f was corrected taking into account the unblocked area for recombination provided by the difference in R_{rec} shown in Fig. 5(a) (a 70%). With this approximation, a donor density of 2.9×10^{21} cm^{-3} was estimated, Table 1.

Even at lower Ga concentration, doping is very high and nearly constant (within the errors arising from the estimation), a result which is in good agreement with high values of conductivity and thus the observation of negligible transport resistance in the semiconductor. It is remarkable that the rise of the estimated donor density does not follow linearly the Ga addition during the synthesis of the nanoparticles. This result suggests that the substitution of Zn^{2+} ions in the ZnO lattice with Ga^{3+} ions effectively acting as donors in ZnO [22,40], saturates at levels around 3×10^{21}. As indicated above, the excess Ga is segregated to the surface and these data suggest that the segregation starts even at levels below 3% Ga addition.

Note that the point at 0.4 V for ZnO:Ga 1% and the points at 0.2 V for ZnO:Ga 3% and 5% were not considered for Mott–Schottky fits of the film capacitance. The first was discarded as it had a strong influence from surface traps capacitance [41,42] as explained below with more detail. The others were discarded because at these potentials, data depart from the Mott–Schottky behavior.

3.5. Interpretation of j–V curves from impedance data

Impedance data allow a better understanding of the results obtained for the j–V curves shown in Fig. 5(a) and summarized in Table 1. Once the short-circuit current is determined, the use of both series and recombination resistance data, provides a calculation of the j-V characteristics from the impedance data through [27].

$$j = j_{SC} - \int_0^V \frac{1}{R_{total}} dV, \quad (4)$$

with $R_{total} = R_{series} + R_{rec}$, where the series resistance is given by $R_{Series} = R_{FTO} + R_{Pt}$ as the other contributions are negligible, see Fig. 5(a).

According to previous publications [27,43,44], the parameters that influence FF are current, series resistance and β. Thus, the low value of the photocurrent in pure ZnO explains the highest FF obtained for this sample, may be explained in part as the ohmic resistive losses that influence negatively the FF values are minimized. With respect to the doped samples, the general low values observed herein have to be attributed both to the low β given by the DSCs and to the S shaped pattern of the j–V curves. This particular shape of the curves has been presented in previous papers [41,42,45,46]. In the case of the ZnO:Ga 1%, the additional drop in FF is attributable to the relatively high series resistance found for this sample, and the remarkable S-pattern of this sample, also noted in the values of capacitance and recombination resistance at 0.4 V shown in Fig. 5. Thus at this potential, ZnO:Ga 1% C_F presents a value slightly larger than the tendency line, while R_{rec} presents a value lower than the tendency line effect that has been previously attributed to the presence of surface trap states producing an extra recombination path [41,42].

With respect to the open-circuit voltage, all the values obtained are around 0.79 V, see Table 1. This coincidence seems related to the fact that all the capacitances saturate to a certain value that is a function of the roughness factor. The high electronic density appearing in these conditions does not allow the V_{OC} rising higher than the level of impurities in the semiconductor (pining of the Fermi level). As consequence there is no effect of Ga addition level on V_{OC} since it is defined as the difference between the Fermi level of the electrons in the semiconductor nanostructure and the redox states in the electrolyte. The coincidence of the apparent flat band potential in all the Mott–Schottky plots reinforces this possibility. To what extent E_{Fn} pinning at shallow doping levels determines V_{OC} in this system is not clear from the available data and requires further investigation.

Author's personal copy

4. Conclusions

Differences in the efficiency of ZnO:Ga doped DSC samples is mostly related to the increase of j_{SC} associated with morphological changes: a rise in the roughness factor due to smaller particles size with increasing Ga contents that yielded to a larger dye upload.

One important conclusion of this work is that the capacitance in the doped samples does not correspond to a chemical capacitance but to the depletion of the doped semiconductor surface. From Mott–Schottky plots a doping level >10^{21} was estimated for all doped samples.

Here it has been shown that Ga doping, saturates at levels around 3×10^{21} cm^3, with segregation of the Ga excess which acts as a barrier for recombination. The Ga doping increases the film capacitance until a limit given by the Ga barrier. Finally, the poor fill factor values reported were associated to the low β obtained in the ZnO-based DSCs.

Acknowledgements

The Brazilian team thanks FAPESP, CNPq and CAPES (under project 199/09) for financial support. M.S.G. thanks FAPESP (2009/14713-3) and CNPq (201516/2007-1 and 141215/2006-2) for fellowships and A.S.G. thanks FAPESP (04/14829-8) and CAPES (PDEE 1089/06-4) for scholarships. The Spanish team acknowledges financial support by the projects from ESF and MCIN under HOPE–Consolider-Ingenio 2010, MEC under PHB-2008-040-PC and Generalitat Valenciana under PROMETEO/2009/058.

References

[1] B. O'regan, M. Grätzel, Nature 353 (1991) 737.
[2] P. De Almeida, J. Van Deelen, C. Catry, H. Sneyers, T. Pataki, R. Andriessen, C. Van Roost, J.M. Kroon, Appl. Phys. A: Mater. Sci. Process. 79 (2004) 1819.
[3] S.-M. Paek, H. Jung, Y.-J. Lee, N.-G. Park, S.-J. Hwang, J.-H. Choy, J. Phys. Chem. Solids 67 (2006) 1308.
[4] C.J. Barbé, F. Arendse, P. Comte, M. Jirousek, F. Lenzmann, V. Shklover, M. Grätzel, J. Am. Ceram. Soc. 80 (1997) 3157.
[5] R. Argazzi, N.Y.M. Iha, H. Zabri, F. Odobel, C.A. Bignozzi, Coord. Chem. Rev. 248 (2004) 1299.
[6] M. Grätzel, Prog. Photovolt.: Res. Appl. 8 (2000) 171.
[7] Y. Cao, Y. Bai, Q. Yu, Y. Cheng, S. Liu, D. Shi, F. Gao, P. Wang, J. Phys. Chem. C 113 (2009) 6290.
[8] T. Bessho, S.M. Zakeeruddin, C.-Y. Yeh, E.W.-G. Diau, M. Grätzel, Angew. Chem. Int. Ed. 49 (2010) 6646.
[9] Q. Yu, Y. Wang, Z. Yi, N. Zu, J. Zhang, M. Zhang, P. Wang, ACS Nano 4 (2010) 6032.
[10] S. Nakade, Y. Saito, W. Kubo, T. Kitamura, Y. Wada, S. Yanagida, J. Phys. Chem. B 107 (2003) 8607.
[11] M. Adachi, Y. Murata, J. Takao, J. Jiu, M. Sakamoto, F. Wang, J. Am. Chem. Soc. 126 (2004) 14943.
[12] H.J. Snaith, L. Schmidt-Mende, M. Grätzel, M. Chiesa, Phys. Rev. B: Condens. Matter 74 (2006) 045306.
[13] G. Boschloo, A. Hagfeldt, Acc. Chem. Res. 42 (2009) 1819.
[14] J.H. Kim, B.D. Ahn, C.H. Lee, K.A. Jeon, H.S. Kang, S.Y. Lee, J. Appl. Phys. 100 (2006) 113515.
[15] M.-S. Oh, D.-K. Hwang, Y.-S. Choi, J.-W. Kang, S.-J. Park, C.-S. Hwang, K.I. Cho, Appl. Phys. Lett. 93 (2008) 111905.
[16] A.B.F. Martinson, J.W. Elam, J.T. Hupp, M.J. Pellin, Nano Lett. 7 (2007) 2183.
[17] M. Guo, P. Diao, X. Wang, S. Cai, J. Solid State Chem. 178 (2005) 3210.
[18] C. Lin, H. Lin, J. Li, X. Li, J. Alloys Compd. 462 (2008) 175.
[19] A. Solbrand, K. Keis, S. Södergren, H. Lindström, S.-E. Lindquist, A. Hagfeldt, Solar Energy Mater. Solar Cells 60 (2000) 181.
[20] K. Keis, J. Lindgren, S.-E. Lindquist, A. Hagfeldt, Langmuir 16 (2000) 4688.
[21] R. Katoh, A. Furube, T. Yoshihara, K. Hara, G. Fujihashi, S. Takano, S. Murata, H. Arakawa, M. Tachiya, J. Phys. Chem. B 108 (2004) 4818.
[22] A.S. Gonçalves, S.A.M. Lima, M.R. Davolos, S.G. Antônio, C.O. Paiva-Santos, J. Solid State Chem. 179 (2006) 1330.
[23] A.H. Jayatissa, Semicond. Sci. Technol. 18 (2003) L27.
[24] A.S. Gonçalves, M.R. Davolos, N. Masaki, S. Yanagida, S. Mori, A.F. Nogueira, J. Appl. Phys. 106 (2009) 064316.
[25] M. Grätzel, Nature 414 (2001) 338.
[26] J. Bisquert, F. Fabregat-Santiago, I. Mora-Seró, G. Garcia-Belmonte, E.M. Barea, E. Palomares, Inorg. Chim. Acta 361 (2008) 684.
[27] F. Fabregat-Santiago, J. Bisquert, E. Palomares, L. Otero, D. Kuang, S.M. Zakeeruddin, M. Grätzel, J. Phys. Chem. C 111 (2007) 6550.
[28] Q. Wang, S. Ito, M. Gratzel, F. Fabregat-Santiago, I. Mora-Sero, J. Bisquert, T. Bessho, H. Imai, J. Phys. Chem. B 110 (2006) 25210.
[29] J. Bisquert, M. Grätzel, Q. Wang, F. Fabregat-Santiago, J. Phys. Chem. B 110 (2006) 11284.
[30] F. Fabregat-Santiago, J. Bisquert, G. Garcia-Belmonte, G. Boschloo, A. Hagfeldt, Solar Energy Mater. Solar Cells 87 (2005) 117.
[31] A.S. Gonçalves, M.R. Davolos, N. Masaki, S. Yanagida, A. Morandeira, J.R. Durrant, J.N. Freitas, A.F. Nogueira, Dalton Trans. (2008) 1487.
[32] K. Keis, L. Vayssieres, H. Rensmo, S.-E. Lindquist, A. Hagfeldt, J. Electrochem. Soc. 148 (2001) A149.
[33] Iupac, Compendium of Chemical Terminology, Iupac, 1997.
[34] K.D. Benkstein, N. Kopidakis, J. Van De Lagemaat, A.J. Frank, J. Phys. Chem. B 107 (2003) 7759.
[35] J. Bisquert, G. Garcia-Belmonte, F. Fabregat-Santiago, A. Compte, Electrochem. Commun. 1 (1999) 429.
[36] F. Fabregat-Santiago, G. Garcia-Belmonte, J. Bisquert, P. Bogdanoff, A. Zaban, J. Electrochem. Soc. 150 (2003) E293.
[37] J. Bisquert, Phys. Chem. Chem. Phys. 5 (2003) 5360.
[38] A.B.F. Martinson, M.S. Goes, F. Fabregat-Santiago, J. Bisquert, M.J. Pellin, J.T. Hupp, J. Phys. Chem. A 113 (2009) 4015.
[39] I. Mora-Seró, F. Fabregat-Santiago, B. Denier, J. Bisquert, R. Tena-Zaera, J. Elias, C. Lévy-Clément, Appl. Phys. Lett. 89 (2006) 203117.
[40] A.E. Suliman, Y. Tang, J. Appl. Sci. 7 (2007) 314.
[41] T.C. Li, M.S. Goes, F. Fabregat-Santiago, J. Bisquert, P.R. Bueno, C. Prasittichai, J.T. Hupp, T.J. Marks, J. Phys. Chem. C 113 (2009) 18385.
[42] I.N. Mora-Seroĭ, S. GimeĭNez, F. Fabregat-Santiago, R. GoĭMez, Q. Shen, T. Toyoda, J. Bisquert, Acc. Chem. Res. 42 (2009) 1848.
[43] S.M. Sze, Physics of Semiconductor Devices, John Wiley and Sons, New York, 1981.
[44] N. Koide, A. Islam, Y. Chiba, L. Han, J. Photochem. Photobiol. A: Chem. 182 (2006) 296.
[45] P. Suri, R.M. Mehra, Solar Energy Mater. Solar Cells 91 (2007) 518.
[46] L. Lu, R. Li, K. Fan, T. Peng, Solar Energy 84 (2010) 844.